GAUSSIAN APPROXIMATIONS FOR ENERGY-BASED DETECTION AND LOCALIZATION IN SENSOR NETWORKS

Volkan Cevher[*] *and Rama Chellappa*

Institute for Advanced Computer Studies,
University of Maryland,
College Park, MD 20742.
{volkan, rama}@umiacs.umd.edu

James H. McClellan

Center for Signal and Image Processing
Georgia Institute of Technology,
Atlanta GA 30332.
jim.mcclellan@ece.gatech.edu

ABSTRACT

Energy-based detection and estimation are crucial in sensor networks for sensor localization, target tracking, etc. In this paper, we present novel Gaussian approximations that are applicable to general energy-based source detection and localization problems in sensor networks. Using our approximations, we derive receiver operating characteristics curves and Cramer-Rao bounds, and we provide a factorized variational Bayes approximation to the location and source energy posterior for centralized or decentralized estimation. When the source signal and the sensor noise have uncorrelated Gaussian distributions, we demonstrate that the envelope of the sensor output can be accurately modeled with a multiplicative Gaussian noise model, which results in smaller estimation biases than the other Gaussian models typically used in the literature. We also prove that additive Gaussian noise models result in negatively biased speed estimates under the same signal assumptions, which can be circumvented by the proposed approximations.

Index Terms— Chi distribution, variational Bayes, energy based detection and localization

1. INTRODUCTION

Energy-based detection and localization (EBDL) are important problems for sensor networks and pose interesting challenges for statistical signal processing. The objective in these problems is the detection, localization, and tracking of an object based on the received energy measurements at spatially distributed sensors. As the energy of the signal is easy to compute and does not require high bandwidth or accurate synchronization to transmit, EBDL has become quite popular in sensor networks [1].

In this paper, we provide general Gaussian approximations of the Chi distribution, which have applications to the EBDL problems. Specifically, we provide approximations of the received root-mean-squared of the signal power based on the Laplacian method [2] and moment matching, and compare the resulting expressions with other approximations typically used in the literature [3, 4, 5]. We also provide simplified receiver operating characteristics (ROC) expressions for target detection under the Neyman-Pearson lemma and the Cramer-Rao lower bound (CRLB) for location estimation. Since received signal power jointly depends on the signal energy and the sensor to target distance, we derive a factorized variational Bayes approximation to the joint posterior of the target energy and target location [6, 7]. Our approximation decouples the target energy estimation and localization, which alleviates the tractability of EBDL.

The organization of the paper is as follows. Section 2 introduces the signal model and describes our approximations. Sections 3 and 4 derive the CRLB and ROC curves for the EBDL problems. Section 5 applies the variational Bayes approach to determine a factorized approximation to the energy-based location posterior. Computer simulations are provided in Section 6 followed by an appendix that analyzes the energy based speed estimation bias.

[*]Prepared through collaborative participation in the Advanced Sensors Consortium sponsored by the U. S. Army Research Laboratory under the Collaborative Technology Alliance Program, Cooperative Agreement DAAD19-01-02-0008.

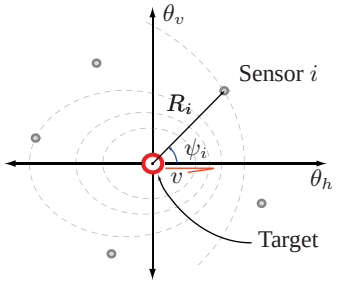

Fig. 1. This figure illustrates the geometry of the sensor-target configuration for a monopole acoustic source moving along the θ_h-direction with a speed of v. The dashed lines are the acoustic wavefronts, which create the interaction between the target and the sensor.

2. SIGNAL MODEL AND DENSITY APPROXIMATIONS

We discuss the power estimation of a narrow-band source using an omnidirectional sensor in an isotropic medium. We assume that there are no multipath effects. We denote $s(t)$, $x(t)$, $n(t)$, and $y(t)$ as the complex envelopes of the source signal, the source signal at the sensor, the sensor additive noise, and the sensor output signal, respectively. The target position is denoted as $\boldsymbol{\theta} = \left[\begin{array}{cc} \theta_h, & \theta_v \end{array}\right]'$ and the position of the sensor as $\boldsymbol{\zeta} = \left[\begin{array}{cc} \zeta_h, & \zeta_v \end{array}\right]'$. Assuming a propagation loss constant α, we write the complex envelope of the sensor output signal at the target narrow band frequency f_0 as follows [8, 9] (see Fig. 1):

$$y(t) = x(t) + n(t) = \frac{s(t)}{\sqrt{\beta} R^{\alpha/2}} e^{-j\frac{2\pi f_0 R}{\beta c}} + n(t), \qquad (1)$$

where R is the range of the source to the sensor, v is the source speed, ψ is the angle of the speed vector with respect to the line connecting the source and the sensor, $\beta = 1 + \frac{v}{c}\cos\psi$ is the Doppler

shift factor, and c is the speed of sound. To calculate the signal power, N snapshots of the acoustic envelopes, calculated at times $(t_1, \ldots, t_N)$, are used. We note that if the time samples are sufficiently apart, then successive samples of the source and the noise samples are uncorrelated [10]. We model the source signal samples as *i.i.d.*, zero mean, complex circularly symmetric Gaussian random variables $\mathcal{CN}\left(0, \sigma_s^2\right)$ with variance σ_s^2 and the noise samples $\mathcal{CN}\left(0, \sigma^2\right)$ with variance σ^2.

Based on our signal and noise assumptions, it is straightforward to prove that the sensor output signal $y(t)$ also has an *i.i.d.* zero mean circularly complex Gaussian distribution with variance $\sigma_y^2 = \sigma_x^2 + \sigma^2$, where $\sigma_x^2 = \frac{\sigma_s^2}{\beta R^\alpha}$. Now, we denote the N-sample root-mean-squared (RMS) output as $\varepsilon = \sqrt{\frac{1}{N}\sum_{i=1}^{N} |y(t_i)|^2}$:

$$\varepsilon = \frac{\sigma_y}{\sqrt{2N}} \sqrt{\sum_{i=1}^{N} \left(\frac{y_{\text{real}}^2(t_i)}{\sigma_y^2/2} + \frac{y_{\text{imag}}^2(t_i)}{\sigma_y^2/2} \right)} = \frac{\sigma_y}{\sqrt{2N}} z, \quad (2)$$

where we define z as the second square-root summation term in (2). The variable z has a Chi distribution $p_Z(z)$ with $2N$ DOF [11]. Then, ε has the following distribution: $\varepsilon \sim p_0(\varepsilon) = \frac{\sqrt{2N}}{\sigma_y} p_Z\left(\frac{\sqrt{2N}}{\sigma_y}\varepsilon\right)$.

In general, we can use $p_0(\varepsilon)$ to determine the target position and a batch of ε measurements to determine the target speed using a constant speed assumption. However, $p_0(\varepsilon)$ is somewhat complex for numerical inference. To facilitate the estimation of range and speed parameters of the target from the received signal power, we make normal approximations to $p_0(\varepsilon)$ using the Laplacian approximation and moment matching (MM). A normal approximation of $p_0(\varepsilon)$ can be determined by approximating $p_Z(z)$ with a Gaussian density $q_Z(z) = \mathcal{N}\left(\mu_z, \sigma_z^2\right)$. Laplacian approximation achieves this by using the mode and the Hessian of the log likelihood at the mode. It is highly accurate even at moderate sample sizes [2]. Moment matching is based on matching the first and the second-order moments of the density of z.

2.1. Laplacian Approximation of ε

The mode of the Chi distribution is given by $\hat{z} = \sqrt{2N-1}$, and the Hessian of the log likelihood of the Chi distribution by

$$L_Z(z) = \frac{\partial}{\partial z^2} \log\left\{ \frac{2^{1-N} z^{2N-1} e^{-z^2/2}}{\Gamma(N)} \right\} = -(2N-1)\frac{1}{z^2} - 1. \quad (3)$$

Laplacian approximation uses $\sigma_z^2 = -1/L_Z(\hat{z})$, resulting in $q_Z(z) \sim \mathcal{N}\left(\sqrt{2N-1}, \frac{1}{2}\right)$.

In turn, ε has the following Gaussian distribution:

$$\varepsilon \approx p_1(\varepsilon) = \mathcal{N}\left(\sqrt{\frac{2N-1}{2N}}\sigma_y, \frac{\sigma_y^2}{4N} \right) \approx \sigma_y e^{\frac{\mathcal{N}(0,1)}{\sqrt{4N}}}, \quad (4)$$

where we used $\sqrt{\frac{2N-1}{2N}} \approx 1$ for $N \gg 1$ and $e^x \approx 1 + x$ for $x \ll 1$. Hence, the RMS output can be approximated with a multiplicative noise model.

2.2. Moment Matching of ε

The mean and the variance of z are given by $\mu_z = \sqrt{2}\frac{\Gamma(N+1/2)}{\Gamma(N)}$ and $\sigma_z^2 = 2N - \mu_z^2$, where $\Gamma(\cdot)$ is the Gamma function [11]. The particular ratio of the Gamma functions in the mean expression has the following series expansion [12]: $\frac{\Gamma(N+1/2)}{\Gamma(N)} =$

$$\sqrt{N}\left(1 - \frac{1}{8N} + \frac{1}{128N^2} + \frac{5}{1024N^3} - \frac{21}{32768N^4} + \ldots\right). \quad (5)$$

In general, $N \gg 1$, hence, we can approximate the ratio as follows:

$$\frac{\Gamma(N+1/2)}{\Gamma(N)} \approx \sqrt{N}\left(1 - \frac{1}{8N}\right) \approx \sqrt{N}\left(1 - \frac{1}{4N}\right)^{0.5} = \sqrt{N - 1/4}. \quad (6)$$

Then, MM results in the following approximation of z: $q_Z(z) \sim \mathcal{N}\left(\sqrt{2N-1/2}, \frac{1}{2}\right)$. This approximation has consistently better scores at different p-values than the Laplacian approximation when tested against Chi distribution. The resulting approximation for ε using MM has the same form as (4) for $N \gg 1$, which is obtained from the Laplacian approximation.

2.3. Other Approximations of ε

In [3], the authors expand ε^2 as

$$\varepsilon^2 = \frac{1}{N}\sum_{i=1}^{N} |x(t_i)|^2 + \frac{2}{N}\Re\sum_{i=1}^{N} x^*(t_i)n(t_i) + \frac{1}{N}\sum_{i=1}^{N} |n(t_i)|^2, \quad (7)$$

and then ignore $\sum_{i=1}^{N} x^*(t_i)n(t_i)$, and invoke the central limit theorem on $\frac{1}{N}\sum_{i=1}^{N} |n(t_i)|^2 \approx \mathcal{N}\left(\sigma^2, \frac{\sigma^4}{2N}\right)$ to arrive at

$$\varepsilon^2 \sim p_2(\varepsilon^2) = \mathcal{N}\left(\sigma_x^2 + \sigma^2, \frac{\sigma^4}{2N}\right) = \mathcal{N}\left(\sigma_y^2, \frac{\sigma^4}{2N}\right). \quad (8)$$

Compared to Laplacian and moment matching approximations, we note that (i) the authors ignore the middle term in (7), which contributes to the total variance, (ii) the Chi-squared distribution reaches normality slower than the Chi distribution, which is problematic when N is small (i.e., $N < 30$) and (iii) the Chi-squared distribution has non zero skewness. Nonetheless, this approximation is useful when the complex envelope samples of the source signal ($s(t)$'s) (i) do not come from a Gaussian distribution, (ii) are uncorrelated in time, and (ii) are uncorrelated with the noise samples, which are assumed white and Gaussian.

In [5], the authors approximate $\varepsilon \sim p_3(\varepsilon) = \mathcal{N}\left(\sigma_x, \hat{\sigma}_\varepsilon^2\right)$ for target localization problems, where the constant $\hat{\sigma}_\varepsilon$ is assumed independent of σ_x. Other authors also have used this approximation in acoustic speed estimation problems, e.g., [13]. In acoustic speed estimation problems, a batch of consecutive signal power estimates are used along with locally linear motion models to estimate the speed of an acoustically loud target. In these problems, the target's closest-point-of-approach (CPA) is assumed known and the target's signal power is assumed constant. Then, the target speed is determined by fitting an envelope function, which depends on the target speed and the target CPA, to the calculated signal power vs. time from the acoustic data. We specifically mention $p_3(\varepsilon)$ because the speed estimates obtained using the pdf $p_3(\varepsilon)$ have negative biases when the target signal data is generated using (1) (see Appendix A).

3. CRAMER-RAO BOUND FOR POSITION ESTIMATION

In most tracking problems, the signal power σ_s^2 is assumed known, and the target position $\boldsymbol{\theta}$ is estimated using the signal power estimates from multiple sensors [14]. In this section, we analytically derive the Cramer-Rao lower bound for position estimation using our approximate density $p_1(\varepsilon|\boldsymbol{\theta})$ and compare the result to the CRLB derived using $p_0(\varepsilon|\boldsymbol{\theta})$. Note that with the known signal power σ_s^2 assumption, ε is a sufficient statistics for the parameter estimation problem, as the knowledge of ε and σ_s^2 completely characterizes the statistical distribution of $s(t)$. Hence, we emphasize that the resulting CRLB expression from $p_0(\varepsilon|\boldsymbol{\theta})$ is the same as the CRLB expression in [14], which is derived using the envelope outputs $s(t)$ directly.

The CRLB for $\boldsymbol{\theta}$ can be obtained by taking the inverse of the Fisher information matrix (FIM) $\boldsymbol{F}(\boldsymbol{\theta})$ [15]. To determine $\boldsymbol{F}(\boldsymbol{\theta})$, we first derive the FIM for range estimation using a single sensor with our approximation $p_1(\varepsilon)$:

$$\boldsymbol{F}_R(R_i) = \int p_1(\varepsilon_i|R_i) \left(\frac{\partial \log p_1(\varepsilon_i|R_i)}{\partial R_i} \right)^2 d\varepsilon_i = \frac{\alpha^2 N \left(\sigma_s^2/\sigma^2\right)^2}{R_i^2 \left(\frac{\sigma_s^2}{\sigma^2} + R_i^\alpha \right)^2}. \tag{9}$$

where it is assumed that $\sqrt{\beta} \approx 1$. The ignorance of the Doppler effect is a reasonable assumption up to moderate target speeds. Then, the FIM for position estimation $\boldsymbol{\theta}$ using a single sensor is given by $F_i(\boldsymbol{\theta}) = \left(\nabla_{\boldsymbol{\theta}} R_i\right) \boldsymbol{F}_R(R_i) \left(\nabla_{\boldsymbol{\theta}} R_i\right)'$, [16]. Assuming *i.i.d.* Gaussian noise on the sensors, the FIM for target position is a summation of the individual sensor FIM's:

$$\boldsymbol{F}(\boldsymbol{\theta}) = \sum_{i=1}^{M} F_i(\boldsymbol{\theta}) = \sum_{i=1}^{M} \boldsymbol{F}_R(R_i) \begin{bmatrix} \cos\psi_i \\ \sin\psi_i \end{bmatrix} \times \begin{bmatrix} \cos\psi_i & \sin\psi_i \end{bmatrix}, \tag{10}$$

where M is the number of sensors in the sensor network and ψ_i is their respective bearings (see Fig. 1). It turns out that if we go through the same FIM derivation using $p_0(\varepsilon|\boldsymbol{\theta})$, the final FIM of the target position estimate is the same as (10). This is intuitive as the density approximation $p_1(\varepsilon|\boldsymbol{\theta})$ matches the curvature of the likelihood at its mode, which corresponds to the CRLB for the problem.

Therefore, the CRLB expression in (10) simplifies the calculation of the CRLB bound derived in [14] (Eqn. (5)). Finally, other Cramer-Rao lower bounds for $p_{2,3}(\varepsilon|\boldsymbol{\theta})$ are given in [3, 4] and [5], respectively. In [3], CRLB is derived for multiple targets.

4. RECEIVER OPERATING CHARACTERISTICS

In this section, we describe and quantify decision procedures for acoustic sensors to declare target detections based on microphone power observations. To derive the optimal detection algorithm and its corresponding receiver operating characteristics (ROC) curve, we start with (1) and its assumptions. The binary hypothesis testing problem is then: H_0: $y \sim \mathcal{CN}\left(0, \sigma^2\right)$; H_1: $y \sim \mathcal{CN}\left(0, \sigma^2 + \sigma_x^2\right)$, where the first hypothesis H_0 assumes that the microphone signal is noise only and the second hypothesis H_1 assumes that the microphone signal is noise plus the target signal. It is straightforward to show that the optimal detector is a square-law detector:

$$\sum_{i=1}^{N} |y(t_i)|^2 \underset{H_0}{\overset{H_1}{\gtrless}} \eta, \tag{11}$$

where η is the detector threshold to be determined using the Neyman-Pearson criteria. Note that the detector (11) results in a uniformly most powerful (UMP) test since the decision regions for each hypothesis is independent from σ_x^2. The threshold η is related to the false alarm rate P_f as follows $P_f = P\left(\chi_{2N}^2 > \frac{2\eta}{\sigma^2}\right)$, where χ_N^2 is the Chi-squared distribution with N degrees of freedom. The detection probability P_d is then given by $P_d = P\left(\chi_{2N}^2 > \frac{2\eta}{\sigma_y^2}\right)$. Then, the ROC curve can be numerically determined by relating P_d to P_f.

When we use our approximate density $p_1(\varepsilon)$, we can simplify the ROC curve expression for the target detection problem. Note that when $N \gg 1$, we can write $\varepsilon \approx \sigma_y + \frac{\sigma_y}{\sqrt{4N}}\mathcal{N}(0,1) \approx \sigma_y e^{\frac{\mathcal{N}(0,1)}{\sqrt{4N}}}$. Denoting $\mathcal{E} = \log \varepsilon$, we have

$$\mathcal{E} \approx p_1(\mathcal{E}) \sim \mathcal{N}\left(\log \sigma_y, \frac{1}{4N}\right) \tag{12}$$

with the following hypotheses: H_0: $\sigma_y = \sigma_n$; H_1: $\sigma_y = \sqrt{\sigma^2 + \sigma_x^2} > \sigma_n$. In this case, the detector is a simple linear threshold detector:

$$\mathcal{E} \underset{H_0}{\overset{H_1}{\gtrless}} \eta', \tag{13}$$

and is also uniformly most powerful (UMP) [16, 15]. It is easy to verify that the ROC curve is determined by

$$P_d = Q\left(Q^{-1}\left(P_f\right) - \sqrt{N}\left(\log(\sigma^2 + \sigma_x^2) - \log\sigma^2\right)\right), \tag{14}$$

where $Q(\cdot)$ is one minus the cumulative distribution function of $\mathcal{N}(0,1)$-random variable, P_d and P_f are the detection and false alarm probabilities, respectively.

Acoustic Arrays: Using the approximate pdf $p_1(\varepsilon)$, we can derive a similar detector algorithm for acoustic arrays, consisting of multiple tethered acoustic microphones. To derive the ROC curves for bearing sensors, we use the following detector:

$$\max_m \mathcal{E}_m \underset{H_0}{\overset{H_1}{\gtrless}} \eta, \tag{15}$$

where $\mathcal{E}_m = \log \varepsilon_m$ for the mth microphone. Probability that the maximum of M statistically independent Gaussian random variables $\mathcal{E}_m$ with the mean $\log\sigma^2$ and variance $\frac{1}{4N}$ exceeds the threshold η is given by $P_f = 1 - \left[1 - Q\left(\sqrt{4N}\left(\eta - \log\sigma\right)\right)\right]^M$.

Similarly, the detection probability can be derived the same way, resulting in the following ROC curve for acoustic arrays for energy-based detection: $P_d =$

$$1 - \left[1 - Q\left(Q^{-1}\left((1-P_f)^{\frac{1}{M}}\right) - \sqrt{N}\left(\log(\sigma^2 + \sigma_x^2) - \log\sigma^2\right)\right)\right]^M. \tag{16}$$

5. FACTORIZED POSTERIOR APPROXIMATIONS

In the acoustic target localization problem, the objective of the sensor network is to determine the target location $\boldsymbol{\theta}$, which is entangled with the target signal power σ_s^2 via (1). In this section, we address the joint estimation of these latent variables, which is summarized as a graphical model in Fig. 2. Instead of using the complex envelope samples $\{s_i(t)\}_{t_1}^{t_N}$, we only use the sufficient statistics $\mathcal{E}_i$ from each sensor i, which can completely determine the distribution of $s_i(t)$ given σ_s^2 and $\boldsymbol{\theta}$. We assume that only the sensors with high *SNR* are contributing to the estimation ($\sigma_s^2/R^2 \gg \sigma^2$), and that the propagation loss constant is $\alpha = 2$. To increase the tractability of the solution for the latent variables $\boldsymbol{\theta}$ and σ_s, we propose using a factorized approximation to the joint posterior distribution of these variables as $p(\mathcal{E}_1, \ldots, \mathcal{E}_M, \sigma_s, \boldsymbol{\theta}) = f_{\sigma_s}(\sigma_s) f_{\boldsymbol{\theta}}(\boldsymbol{\theta})$. The construction of our approximation follows the factorized variational Bayesian (VB) approximations commonly used in the literature [6, 7].

Under the mean field theory framework, we consider minimizing the Kullback-Leibler (KL) divergence of the full posterior $p_1(\boldsymbol{\mathcal{E}}, \sigma_s, \boldsymbol{\theta})$ from our factorized approximation $f_{\sigma_s}(\sigma_s) f_{\boldsymbol{\theta}}(\boldsymbol{\theta})$ [6, 7], where $\boldsymbol{\mathcal{E}} = [\mathcal{E}_1, \ldots, \mathcal{E}_M]$. Then, the optimal factors f^*'s can be determined from the following implicit expressions:

$$f_{\sigma_s}^*(\sigma_s) \propto \exp\left(E_{\boldsymbol{\theta}} \log p_1(\boldsymbol{\mathcal{E}}, \sigma_s, \boldsymbol{\theta})\right), \; f_{\boldsymbol{\theta}}^*(\boldsymbol{\theta}) \propto \exp\left(E_{\sigma_s} \log p_1(\boldsymbol{\mathcal{E}}, \sigma_s, \boldsymbol{\theta})\right). \tag{17}$$

Note that (17) does not represent an explicit solution as the solutions of the optimal factors depend on expectations computed with respect to other factors. Therefore, (17) denotes a set of consistency conditions, which can be cycled to reach a consensus. It can be shown that convergence is guaranteed [6, 7].

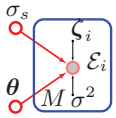

Fig. 2. A directed acyclic graph is used to represent the inference problem, where the box denotes the set of M acoustic sensor observations $\mathcal{E}_i$, which are assumed independent. The deterministic (known) components of the problem are shown with solid dots. The shaded node represents the observed variables $\mathcal{E}_i$, whereas the remaining nodes represents the latent variables σ_s and $\boldsymbol{\theta}$.

From the graphical model in Fig. 2, the posterior density factors as $p(\boldsymbol{\mathcal{E}}, \sigma_s, \boldsymbol{\theta}) = p(\sigma_s)p(\boldsymbol{\theta}) \prod_{i=1}^{M} p_1(\mathcal{E}_i|\sigma_s, \boldsymbol{\theta})$, where $p_1(\cdot)$ is our approximation in (12), and $p(\sigma_s)$ and $p(\boldsymbol{\theta})$ are prior distributions for σ_s and $\boldsymbol{\theta}$. We use the following conjugate prior distributions:

$$p(\sigma_s) \sim \text{Log-}\mathcal{N}\left(\mu_0, \upsilon_0^2\right);\ p(\boldsymbol{\theta}) \sim \mathcal{N}\left(\boldsymbol{\theta}_0, \boldsymbol{\Sigma}_0\right). \tag{18}$$

Note that the posterior density does not factorize directly in terms of σ_s and $\boldsymbol{\theta}$. When the target signal *SNR* is high, the posterior log-likelihood can be approximated by the following expression:

$$\log p(\boldsymbol{\mathcal{E}}, \sigma_s, \boldsymbol{\theta}) = -2N \sum_{i=1}^{M} (\mathcal{E}_i - \log \sigma_s + \log R_i)^2 - \frac{(\log \sigma_s - \mu_0)^2}{2\upsilon_0^2} - \log \sigma_s - \frac{1}{2}(\boldsymbol{\theta} - \boldsymbol{\theta}_0)' \boldsymbol{\Sigma}_0^{-1} (\boldsymbol{\theta} - \boldsymbol{\theta}_0). \tag{19}$$

Now, we describe the VB cycles starting with σ_s. From (17), (18), and (19), it is easy to obtain that $f_{\sigma_s}^{\{1,1:M\}} \sim \text{Log-}\mathcal{N}\left(\mu_1, \upsilon_1^2\right)$, where

$$\upsilon_1^2 = \left(4NM + \upsilon_0^{-2}\right)^{-1},\ \mu_1 \approx \mu_0 \frac{\upsilon_1^2}{\upsilon_0^2} + 4N\upsilon_1^2 \sum_{i=1}^{M} (\mathcal{E}_i + \log|\boldsymbol{\theta}_0 - \boldsymbol{\zeta}_i|). \tag{20}$$

To obtain (20), we approximate $E_{\boldsymbol{\theta}} \log R_i \approx \log|\boldsymbol{\theta}_0 - \boldsymbol{\zeta}_i|$.

The VB cycle on $\boldsymbol{\theta}$ cannot be rearranged into a Gaussian form: $\log f_{\boldsymbol{\theta}}^{\{1,1:M\}}(\boldsymbol{\theta}) = -2N \sum_{i=1}^{M} (\mathcal{E}_i - \mu_1 + \log R_i)^2 - \frac{1}{2}(\boldsymbol{\theta} - \boldsymbol{\theta}_0)' \boldsymbol{\Sigma}_0^{-1} (\boldsymbol{\theta} - \boldsymbol{\theta}_0)$. Since it requires too much computation to numerically obtain the Gaussian approximation directly from the KL divergence, we approximate this VB cycle with a Laplacian approximation: $f_{\boldsymbol{\theta}}^{\{1,1:M\}}(\boldsymbol{\theta}) \sim \mathcal{N}(\boldsymbol{\theta}_1, \boldsymbol{\Sigma}_1)$, where

$$\boldsymbol{\Sigma}_1^{-1} \approx \boldsymbol{\Sigma}_0^{-1} + \sum_{i=1}^{M} \frac{4N}{R_i^2} \begin{bmatrix} \cos\psi_i \\ \sin\psi_i \end{bmatrix} \times \begin{bmatrix} \cos\psi_i & \sin\psi_i \end{bmatrix}, \tag{21}$$

and $\boldsymbol{\theta}_1$ is the maximizer of $\log f_{\boldsymbol{\theta}}^{\{1,1:M\}}(\boldsymbol{\theta})$. We continue the VB cycles by treating $f_{\sigma_s}^{\{k-1,1:M\}}$ and $f_{\boldsymbol{\theta}}^{\{k-1,1:M\}}$ as priors and repeating (20) and (21) for $k = 1, \ldots, K$ to obtain $f_{\sigma_s}^{\{K,1:M\}}$ and $f_{\boldsymbol{\theta}}^{\{K,1:M\}}$ or until they converge, whichever comes first.

The processing of the VB cycles can be distributed, where local message passing is used. As an example, assume that the sensor triplets are ordered and there is a known communication path with a chain structure. The first triplet in the chain starts with the conjugate priors and does its own VB cycle to obtain $f_{\sigma_s}^{\{K',1\}}$ and $f_{\boldsymbol{\theta}}^{\{K',1\}}$, where $K' = 3K/M$. The second triplet in the chain takes the result of first triplet as prior and determines $f_{\sigma_s}^{\{2K',1:2\}}$ and $f_{\boldsymbol{\theta}}^{\{2K',1:2\}}$. This propagation is continued up to the last triplet that obtains $f_{\sigma_s}^{\{MK',1:M/3\}}$ and $f_{\boldsymbol{\theta}}^{\{MK',1:M/3\}}$, which is propagated back to all the triplets in the chain. When compared to the full VB cycles that use the data from all sensors, the distributed implementation is more susceptible to local minima problems.

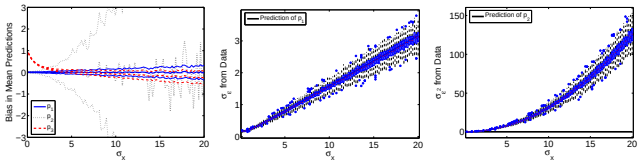

(a) (b) (c)

Fig. 3. (a) Bias in the mean estimates ($\pm$ 1-standard deviation). (b) Standard deviation of ε around its mean (boxplot) vs. the estimate by $p_1(\varepsilon)$. (c) Standard deviation of ε^2 around its mean (boxplot) vs. the estimate by $p_2(\varepsilon)$.

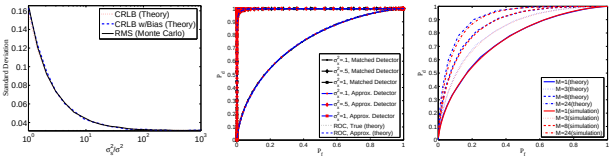

(a) (b) (c)

Fig. 4. (a) Range estimation performance (single sensor). (b) ROC curve (single sensor). (c) ROC curve (acoustic array).

6. SIMULATIONS

Figure 3 compares the estimation performance of the approximate pdf's p_i ($i = 1, 2, 3$) with a Monte Carlo simulation of (1) having following parameters: $N = 10$ and $\sigma^2 = 1$. We estimated the variance estimates in experiments with 100 trials, whose variances were obtained by repeating each trial 100 times. Figure 3 shows that among the approximate pdf's, p_1 (MM) is the best because (i) it has the least bias in the mean estimation of ε with minimum variance and (ii) it follows the actual variance of the data correctly. The variance estimates of p_2 and p_3 are not correct because σ_ε and σ_{ε^2} are not constant and increase with σ_x as shown in Figs. 3(b) and (c). As N gets larger, the variance of the mean estimate bias of p_3 decreases; however, it is quite slow.

Figure 4(a) shows the range estimate results of a Monte Carlo simulation of (1) with the following parameters: $R = 2$m, $N = 1000$, and 10^5 trials. The estimator is given by $\hat{R} = \frac{\sigma_s}{\sqrt{\varepsilon^2 - \sigma^2}}$, when ε is greater than a threshold to ensure a false alarm rate of 1%. The dotted line is calculated taking the square root of the inverse of FIM in (9), whereas the dashed line is calculated by incorporating the bias terms in the the information inequality (it is possible to determine the gradient of bias). Both curves follow the estimated RMS error closely. Another Monte Carlo run of (1) is done with $\sigma^2 = 1$ and $N = 100$ to compare the performances of the alternative approaches for target detection based on microphone outputs (Figs. 4(b) and (c)). We note that the theoretical ROC curves (Chi-squared detector: dotted line, our Gaussian approximation: dashed line) are indistinguishable from the simulation results and are very close. Figure 4(c) shows that the detection performance of sensors with multiple microphones can be accurately predicted with our approximation (16) ($\sigma^2 = 1$, $\sigma_x^2 = 0.1$, and $N = 100$).

Figures 5(a)-(c) illustrate the results of a Monte-Carlo run that compares the VB estimation algorithm with the ML. We simulated a network of 5 acoustic sensors to determine the location of a target situated at $[-3, -3]$. For the target location and power prior, we used $p(\boldsymbol{\theta}_0) \sim \mathcal{N}\left([10, 10]', 50^2 \boldsymbol{I}\right)$ and $p(\sigma_s) = \text{Log-}\mathcal{N}\left(0.5 \log \mathit{SNR}, 10^{-1}\right)$.

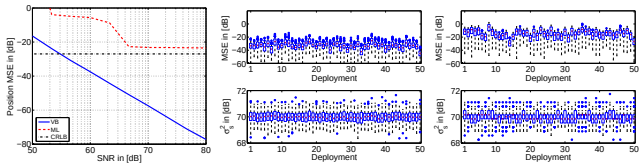

(a) MSE vs. SNR (b) VB @ 70dB (c) ML @ 70dB

Fig. 5. (a) Performance comparison of VB and ML. (b) and (c) show a realization at *SNR* $= 70$dB, which is a typical *SNR* for commercial vehicles. Although the σ_s^2 estimation performance is similar, the VB has much better localization performance.

The sensors were uniformly distributed on a ring centered at the origin (so that the sensor locations is not symmetric with respect to the target location) with inner and outer radii of 5 and 50, respectively. During the Monte-Carlo run, we randomly placed the sensors on the ring, then by fixing the *SNR* at a constant value, we simulated (1) 100 times with $N = 100$ and $\sigma^2 = 1$, and estimated the target position using the VB cycles outlined in Sect. 5 and the ML estimation. The ML estimate maximizes the following likelihood $\log p(\boldsymbol{\mathcal{E}}|\sigma_s, \boldsymbol{\theta}) = -2N \sum_{i=1}^{M} (\mathcal{E}_i - \log \sigma_s + \log R_i)^2$ over the three dimensional space of $[\sigma_s^2; \boldsymbol{\theta}]$. During the simulation, we varied the SNR for the same target positions. Subsequently, different sensor deployments were realized 50 times. For the ML estimates, a grid search over the target *SNR* is used whereas the position is determined using interior point methods for each *SNR*. For the VB cycles, σ_s is initialized to a realization from Log-$\mathcal{N}\left(0.5 \log \mathit{SNR}, 10^{-1}\right)$ (which perturbs σ_s^2 within ± 3dB), whereas the target position is set to $[10, 10]'$. We used a total of 40 VB cycles.

Figure 5(a) shows that the VB method beats the unbiased CRLB and continues to improve as *SNR* increases, whereas the ML method saturates at the bound. This is not a contradiction as we used the unbiased version of the information inequality while calculating the CRLB. For other methods that beat the unbiased CRLB for this problem, see [14] (e.g., Fig. 5). The CRLB is calculated by maximizing the FIM over the sensor deployment. Hence, the bound is not tight for the ML curve, which is an average over the sensor deployments. As some of the ML estimates diverged, the ML performance curve has a shoulder between 50-65dB in Fig. 5(a).

7. CONCLUSIONS

In this paper, we provided Gaussian approximation to the Chi distribution, which alleviates the analytical tractability and numerical calculation of ROC curves and Cramer-Rao lower bound (CRLB) for energy-based detection and localization problems. We also provided a factorized variational Bayes (VB) approximation to the joint source energy and location posterior, which effectively decouples the estimation of the source energy and location. The VB framework is quite powerful and we plan to extend our formulations to multiple energy-based target tracking problems.

A. BIAS IN SPEED ESTIMATION

We analyze the speed estimation bias for the estimates of $p_3(\varepsilon)$ when the data is generated by (1). Let $\alpha_k(v)$ denote monotonically decreasing functions of v for all k, e.g., the envelope observations as a function of v, indexed by time k (e.g., Eqn. (11) in [13]). Define two generative models as follows: Model I: $\mathcal{E}_k = \alpha_k(v) + n_k$, Model II: $\mathcal{E}_k = \alpha_k(v) e^{m_k}$, where n_k and m_k are *i.i.d.* zero mean Gaussian random variables with variances σ_n^2 and σ_m^2. Let v^* be the true speed and v be the ML estimate of Model I, when $\mathcal{E}_k$ is from Model II:

$$v = \arg\min_v J(v), \; J(v) = \sum_k \left(\mathcal{E}_k - \alpha_k(v)\right)^2, \tag{22}$$

Given a sufficient number of $\mathcal{E}_k$ measurements, we expect the ML solution to be near the true value of v^*. Hence, we can assume $v = v^* + \epsilon$, where $\epsilon \ll v^*$ so that $\alpha_k(v) \approx \alpha_k(v^*) + \dot{\alpha}_k(v^*)\epsilon, \forall k$.

The ML estimate of v is found by taking the derivative of $J(v)$ with respect to v. By taking the derivative and equating to zero, we solve for the bias and take its expected value:

$$\epsilon = \frac{\sum_k \dot{\alpha}_k(v^*)\alpha_k(v^*)\left(e^{m_k} - 1\right)}{\sum_k \left[\dot{\alpha}_k(v^*)\right]^2} \Rightarrow \overline{\epsilon} = \frac{\sum_k \dot{\alpha}_k(v^*)\alpha_k(v^*)\left(e^{\frac{\sigma_m^2}{2}} - 1\right)}{\sum_k \left[\dot{\alpha}_k(v^*)\right]^2}, \tag{23}$$

which is always negative since $\alpha_k(v) > 0$ is a monotonically decreasing function of v, i.e., $\dot{\alpha}_k(v^*) < 0$. Hence, given v^*, the expected value of the ML estimate of Model I will always have a negative bias when the data is generated by Model II.

B. REFERENCES

[1] I. F. Akyildiz, W. Su, Y. Sankarasubramaniam, and E. Cayirci, "A survey on sensor networks," *IEEE Communications Magazine*, vol. 40, no. 8, pp. 102–114, 2002.

[2] L. Tierney and J. B. Kadane, "Accurate approximations for posterior moments and marginal densities," *Journal of the American Statistical Association*, , no. 81, pp. 82–86, 1986.

[3] X. Sheng and Y. H. Hu, "Energy based acoustic source localization," in *IPSN*, 2003, pp. 285–300.

[4] D. Li and Y. H. Hu, "Energy-based collaborative source localization using acoustic microsensor array," *EURASIP Journal on Applied Signal Processing*, vol. 2003, no. 4, pp. 321–337, 2003.

[5] J. Liu, X. Koutsoukos, J. Reich, and F. Zhao, "Sensing field: coverage characterization in distributed sensor networks," in *ICASSP 2003*, vol. 5, pp. 173–176.

[6] M. I. Jordan, Z. Ghahramani, T. S. Jaakkola, and L. K. Saul, "An introduction to variational methods for graphical models," *Machine Learning*, vol. 37, no. 2, pp. 183–233, 1999.

[7] C. M. Bishop, *Pattern recognition and machine learning*, Springer, 2006.

[8] P. Morse and K. Ingard, *Theoretical Acoustics*, McGraw-Hill, 1968.

[9] K. L. Bell, Y. Ephraim, and H. L. Van Trees, "Explicit Ziv-Zakai lower bound for bearing estimation," *IEEE Transactions on Signal Processing*, vol. 44, no. 11, pp. 2810–2824, 1996.

[10] W. B. Davenport II and W. L. Root, *An Introduction to the Theory of Random Signals and Noise*, New York: McGraw-Hill, 1958, ch. 6, sec. 6-4, pp. 93–96.

[11] M. Evans, N. Hastings, and B. Peacock, *Statistical distributions. Ed*, Wiley & Sons. New York, 2000.

[12] R. L. Graham, D. E. Knuth, and O. Patashnik, "Concrete mathematics: a foundation for computer science," 1989.

[13] C. Couvreur and Y. Bresler, "Doppler-based motion estimation for wide-band sources from single passive sensor measurements," in *ICASSP 1997*, 21–24 April 1997.

[14] T. Pham, B. M. Sadler, and H. Papadopoulos, "Energy-based source localization via ad-hoc acoustic sensor network," in *IEEE Workshop on Statistical Signal Processing*, 2003, pp. 387–390.

[15] E. L. Lehmann and G. Casella, *Theory of Point Estimation*, Springer, 1998.

[16] H. L. Van Trees, *Detection, Estimation, and Modulation Theory, Part I*, John Wiley & Sons, Inc., 1968.